STRESS CORROSION CRACKING

OF

LAC DU BONNET GRANITE IN TENSION AND COMPRESSION

by

Larry P. Bielus

A thesis
presented to the University of Manitoba
in partial fulfillment of the
requirements for the degree of
Master of Science
in
Civil Engineering

Winnipeg, Manitoba, 1988

STRESS CORROSION CRACKING OF LAC DU BONNET GRANITE

IN TENSION AND COMPRESSION

BY

LARRY P. BIELUS

A thesis submitted to the Faculty of Graduate Studies of
the University of Manitoba in partial fulfillment of the requirements
of the degree of

MASTER OF SCIENCE

© 1988

I hereby declare that I am the sole author of this thesis.

I authorize the University of Manitoba to lend this thesis to other institutions or individuals for the purpose of scholarly research.

Larry P. Bielus

I further authorize the University of Manitoba to reproduce this thesis by photo copying or by other means, in total or in part, at the request of other institutions or individuals for the purpose of scholarly research.

Larry P. Bielus

ABSTRACT

Rocks subjected to long term loading have been known to suffer microcracking. The rate of cracking is sensitive to the applied stress, tensile or compressive, the magnitude of stress relative to the instantaneous strength and the environmental conditions including temperature and moisture.

For tensile loading, the sensitivity of granite to time dependent cracking is demonstrated using the double torsion test. The crack velocity versus stress intensity function is established for three environments, dry (room temperature and 25 percent humidity), wet (room temperature and 100 percent humidity) and hot wet (90 degrees celsius and 100 percent humidity).

For compressive loading, time dependent cracking is evaluated from uniaxial compressive creep tests conducted in the dry and wet environments. The rate of cracking is defined by the relationship between the crack growth rate, expressed as the crack volume strain rate, and the uniaxial compressive stress.

The crack volume strain rate versus stress function has been integrated to obtain a lifetime estimate for Lac du Bonnet Granite. After 1000 years of loading in uniaxial compression at room temperature and 100 percent humidity, the strength of this granite could reduce from 225 MPa to 90 MPa.

ACKNOWLEDGEMENTS

TABLE OF CONTENTS

LIST OF TABLES

LIST OF FIGURES

1.0 INTRODUCTION

The disposal of nuclear waste in geologic repositories is
being extensively researched throughout the world. Canada in
particular is concentrating its research efforts on granitic
plutons situated within the Canadian Shield (Boulton, 1978).
The locations of the Canadian Shield plutons are attractive
because the Shield is centrally located and forms over 50% of
the Canadian landmass. These plutons are considered to be
ideal receptacles for the storage of nuclear waste due to
their nominally unfractured character and their long term
stability over billions of years.

One of the major concerns with using granitic rocks for a
waste repository is the influence of natural discontinuities
and how they could affect the performance of the repository
with time. The growth of microcracks in the intact rock due
to long term loading could add to the porosity of the rock
around the repository. The zone of cracked rock in turn could
connect with the natural fracture system and thus facilitate
the dispersion of toxic wastes through groundwater flow.

In the vicinity of a nuclear waste repository elevated
temperatures, high moisture levels and increased stress levels
would occur. The short term effects of these factors on the
deformation and strength of rocks is generally mechanical,

1

however over the long term chemical effects can occur as well. The process of time dependent chemical reactions that affect the strength of rocks is known as stress corrosion cracking. Although the strength of intact granite is one of the highest for rocks, the granite would still be subject to stress corrosion cracking (Anderson, 1977; Kranz, 1980).

This thesis examines the effects of stress corrosion cracking on the fracture of Lac du Bonnet Granite. To simulate time dependent stress corrosion cracking in the vicinity of a nuclear waste repository, crack growth is evaluated under tensile and compressive loading using increasing stress levels and various environmental conditions. A function, relating crack growth rate and uniaxial compressive stress, is defined and used to predict the failure time for Lac du Bonnet Granite under expected conditions of a waste repository.

2.0 GEOLOGY

2.1 LOCATION

The test specimens used in this study were obtained from Cold
Spring Quarry. The quarry is located approximately 17
kilometres south/southwest from the town of Lac du Bonnet,
Manitoba along the southern edge of the Lac du Bonnet
Batholith, as shown on Figure 1.

2.2 GENERAL GEOLOGY

The Lac du Bonnet Batholith is elongate in shape striking
east/northeast. The unit is the youngest and largest pluton
in the area and is 100 kilometres long with an areal extent of
1000 square kilometres. It is a flat, sheet-like intrusion
dipping to the northwest. The main phase of the pluton is
characterized by massively jointed, homogeneous, equigranular,
unfoliated pink quartz monzonite (McRitchie and Weber, 1971).
The batholith has been Potassium-Argon dated at 2495 +/- 130
million years (Penner and Clark, 1971). The surrounding rock
units include the Winnipeg River plutonic complex to the
south, and the Bird River greenstone belt to the northeast
(McRitchie and Weber, 1974).

3
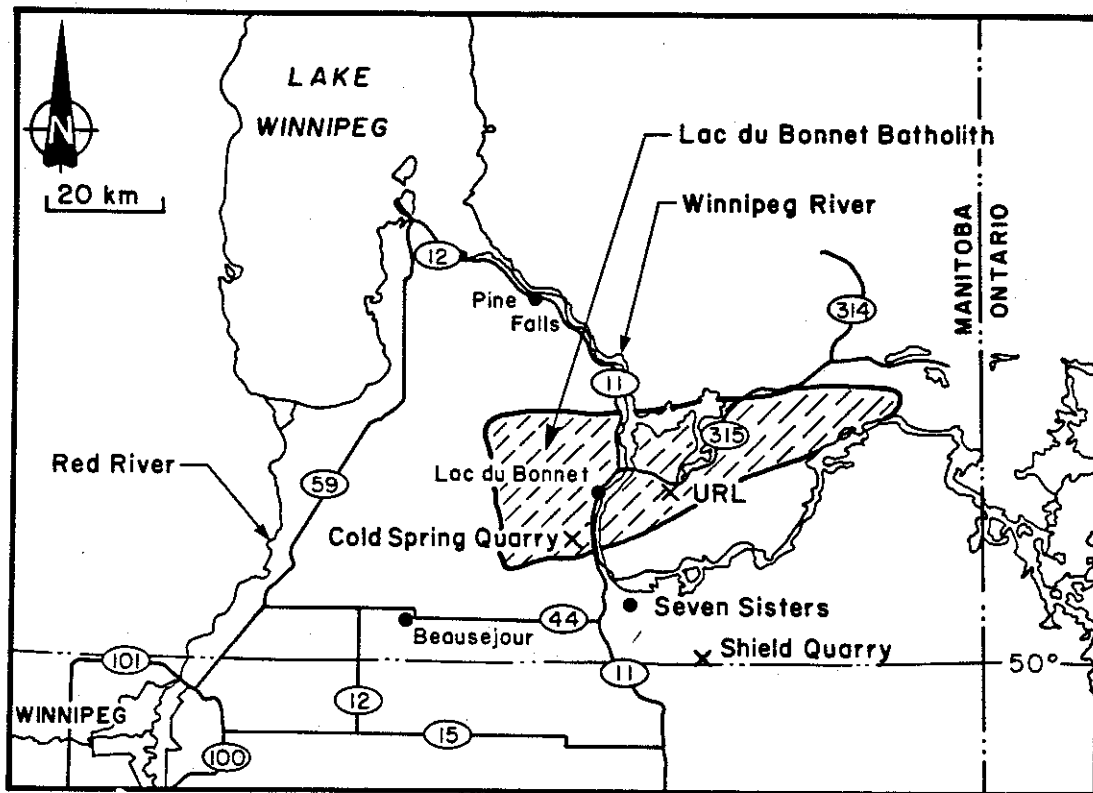
FIGURE 1

LOCATION MAP OF COLD SPRING QUARRY

2.3 PETROLOGY AND MINERALOGY

The mineralogy of the batholith is generally quite simple.
The main phase of the pluton is coarse-grained (0.5 mm - 2.0
cm), and contains quartz, plagioclase (oligoclase), potassium
feldspar (microcline), and biotite. Svab and Lajtai (1981),
described the mineralogy as indicated in Table 1. Minor
accessory minerals include magnetite, apatite, and trace
amounts of zircon. Tammemagi et al (1980), have classified
the batholith as being granitic to granodioritic in
composition. Throughout the remaining text, the Lac du Bonnet
batholith will be referred to as LDB Granite.

TABLE 1

MINERALOGY OF LAC DU BONNET GRANITE

(Svab and Lajtai, 1981)

MINERAL	AVERAGE %
Oligoclase	36
Microcline	31
Quartz	28
Biotite	5

3.0 EXPERIMENTAL PROCEDURE

The fracture of LDB Granite was investigated under tensile loading, using the double torsion test and under compressive loading using the uniaxial compressive creep test. In both tests, time dependent stress corrosion cracking was evaluated under increasing stress levels and various environmental conditions. A description of the two testing procedures is presented in the following sections.

3.1 DOUBLE TORSION TEST

The double torsion test, developed by Kies and Clark (1969), involves torsional loading of a rectangular plate in a simple test apparatus. The test specimens used in this study were plates of LDB Granite, machined 200 mm long, 100 mm wide and 8 mm thick. For all specimens, the 100 mm dimension was parallel to the thickness of the purchased rock slabs obtained from Cold Spring Quarry. Although it has been shown that axis orientation has only a minor influence on rock strength (Svab and Lajtai, 1981), it was desirable to keep this variable constant. A centre notch, 2 mm wide and 20 mm long in the 200 mm direction, was cut into the specimen using a diamond cutting wheel to form a directional starting point for crack propagation. An illustration of the test specimen is presented on Figure 2.
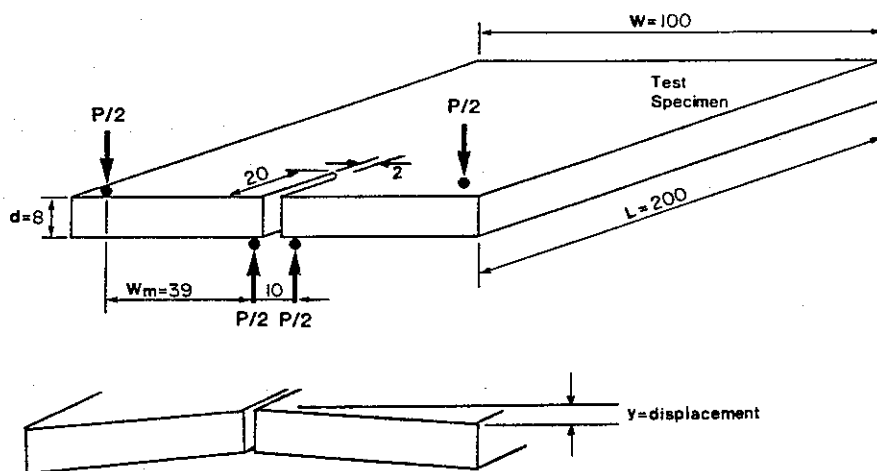
All Dimensions in mm
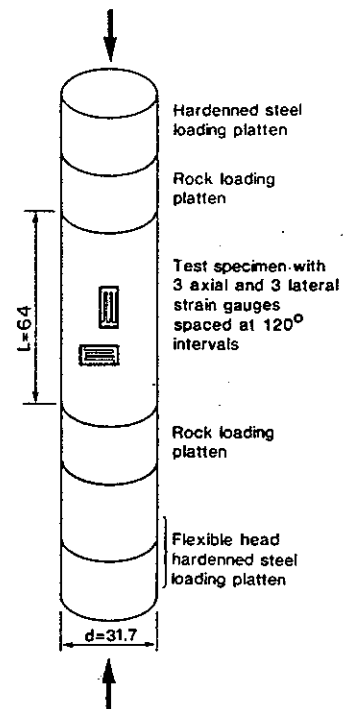
FIGURE 2

SPECIMEN CONFIGURATION AND LOADING ARRANGEMENT FOR THE

DOUBLE TORSION (LEFT) AND COMPRESSION EXPERIMENTS (RIGHT)

A schematic of the testing apparatus used with the double

torsion specimen is shown on Figure 3. The specimen is

supported at the front by two hemispheres located on either

side of the centre notch. A load is transferred through an

upper loading plate to an additional two hemispheres located

on each side of the specimen as illustrated. This arrangement

creates a torsional load on the specimen with moment arms

equal to the distance between the upper and lower loading

points. With this arrangement, only the moment arm width and

the plate thickness are required for data analysis. Rear

supports for the specimen are not critical and were used here

only for convenience in mounting and aligning the test

specimen.

The test apparatus can be used in any loading machine which

has the capacity to transmit compressive displacements and

measure compressive loads. In this study an ELE gear driven

testing machine, capable of hand loading, was used. The

ability to hand load was found extremely beneficial for

obtaining reproducible pre-selected loads during load up. The

pre-selected loads were rapidly applied to the test specimens

(approximately 5 seconds), after which the cross-head

displacement of the loading machine was held constant. The

load was then monitored as a function of time to obtain the

rate of load relaxation. Once load relaxation became

asymptotic, no change in load with time, the test was

8

Specimen

Rear
Supports

Upper Hemisperes

Guide Pins

Lower Hemispheres

Upper Loading
Plate

Lower Loading
Plate
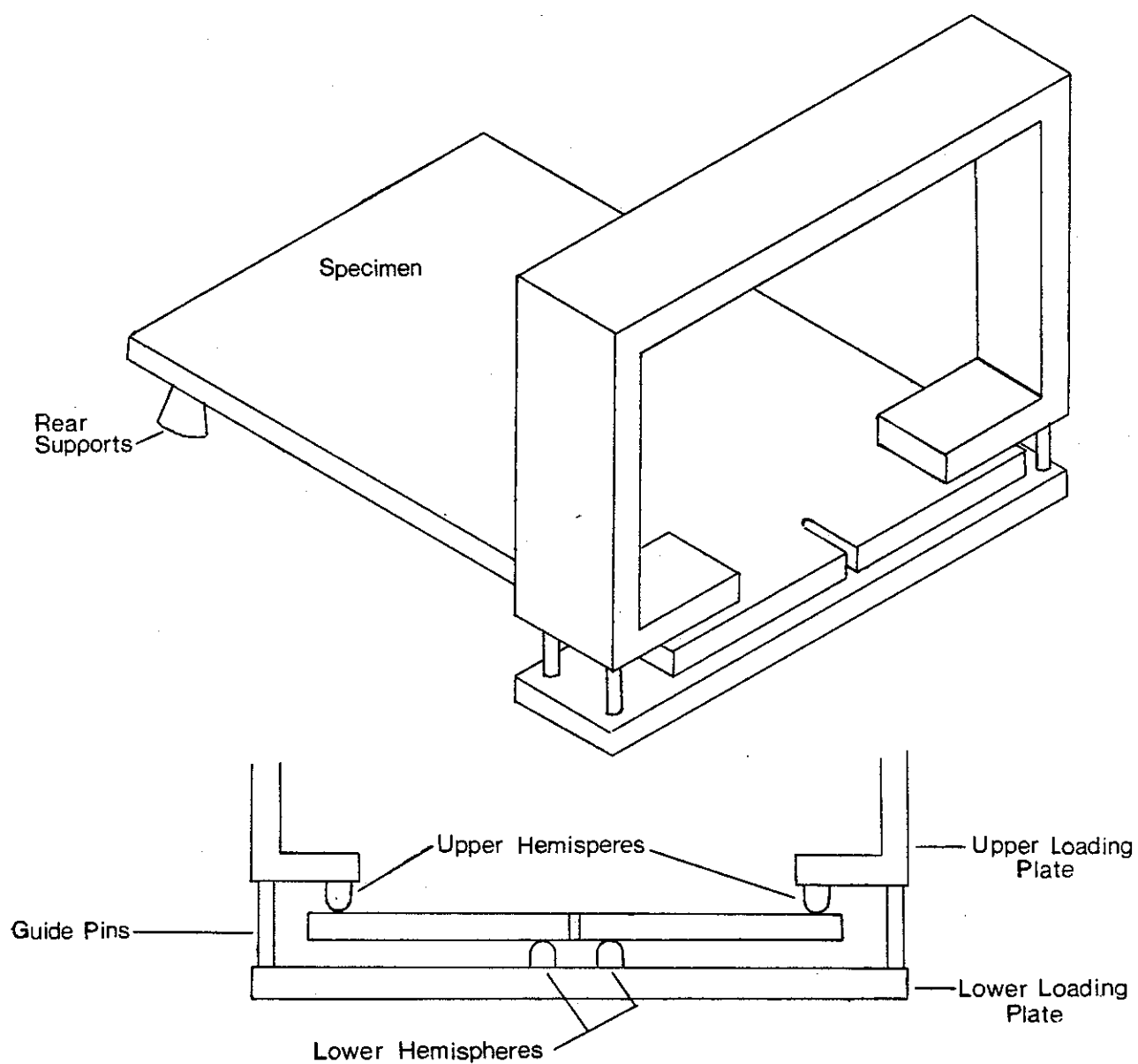
FIGURE 3

SCHEMATIC OF TESTING APPARATUS FOR THE DOUBLE TORSION TEST

considered complete. Additional tests may be completed on the same specimen by simply increasing the cross head displacement to introduce another pre-selected load. It has been determined experimentally that the specimen can be re-used with cracks at least as long as one half of the specimen length (Williams and Evans, 1973).

The simplicity of the double torsion test has several advantages in analyzing fracture under tensile loading. Two of the most noteworthy include the flexibility to test specimens in harsh environmental conditions and the ability to optically examine slow crack growth. To test specimens under varying environmental conditions the testing apparatus was placed within a small stainless steel tank constructed to fit on the compression machine. The tank was connected to a water bath capable of circulating water at various temperatures. To evaluate simulated effects of stress corrosion cracking in a waste repository, tests were conducted in dry, wet and hot wet environments. The dry tests were conducted at room temperature and room humidity which were respectively, approximately 25 degrees celsius and 25 percent relative humidity. The wet tests were completed submerged in water at room temperature and the hot wet tests submerged in water at 90 degrees celsius. Prior to testing in the wet environments, specimens were first placed in a water-filled vacuum desiccator for a 24 hour period to promote initial specimen

saturation. This procedure is based on ASTM standard 564.

A Nikon binocular microscope outfitted with a 35 mm Nikon camera was used under reflected, polarized light to optically view and photograph the specimens. LDB Granite is a polycrystalline, brittle solid in which the major constituent minerals and the grain boundaries between them offer variable degrees of resistance to crack growth. The above arrangement is a useful means to observe, characterize and document their control on crack growth either in-situ, as crack propagation occurs or after, by examining the failed specimen. Thin sections cut from failed and unfailed specimens were also viewed optically using transmitted light microscopy.

3.2 UNIAXIAL COMPRESSIVE CREEP TEST

The test specimens used in the uniaxial compressive creep tests were small cylinders, 31.7 mm in diameter and 64 mm in length. The specimens were cored parallel to the thickness of the granite slabs obtained from Cold Spring Quarry. As with the double torsion specimens it was desirable to keep the axis orientations constant. The drilled core was trimmed with a diamond saw and the ends ground parallel with a diamond impregnated grinding wheel (100 grit size) mounted on a commercial grinding machine. For testing, the granite cylinders were placed between a pair of granite loading

11

platens of the same diameter, followed by hardened steel platens. An illustration of the specimen arrangement is presented on Figure 2.

The test specimens were instrumented with three axially and three laterally orientated 12 mm long MM electric strain gauges glued to the specimen as shown on Figure 2. The strain gauge installations on the specimens which were to be submerged in water for the wet environment testing were waterproofed using the Micromeasurements M-Coat-G Kit. Waterproofing for the underwater strain gauge instrumentation was a difficult, time consuming and chancy exercise. Despite all of the care taken in preparation, over one half of the prepared specimens developed leaks and had to be discarded.

During testing, specimens were used in pairs, one under load and the other (dummy specimen) without load. Both were equally equipped and subjected to the same environmental conditions. A stainless steel chamber connected to a temperature controlled water bath was used to simulate the various environmental conditions, as in the double torsion test. Due to difficulties in maintaining the electronics on the hot wet specimens, only the tests completed in the dry and wet environments were eventually analyzed. When submerged in water, a well waterproofed specimen would show some initial swelling with the strain stabilizing after several days of

soaking.   No vacuum saturation was applied to the specimens.

Once the specimens were prepared the entire arrangement,
including test chamber, was placed into the loading frame for
testing.   The creep tests were conducted using spring loaded
frames manufactured by Soiltest.   The springs are installed in
series with the specimen to minimize load decay due to the
deformation of the specimen and the frame.   In this way, a
constant load could be maintained within +/- 0.5 percent of
the desired load.   The load was applied using a hydraulic jack
pressurized with a hand pump.   Once a week the load had to be
increased to keep within the desired 0.5 percent range.   A
schematic of the loading frame is shown on Figure 4.   To
investigate the microstructural and mineralogical control on
crack propagation under compressive loading, thin sections
were cut from failed and unfailed specimens and viewed
optically using transmitted light microscopy.

THREADED RODS

HYDRAULIC JACK

LEVEL NUTS

CIRCULAR PLATES

LOAD CELL

TO LOAD GAGE

SPRINGS
(FOR CLARITY ONLY
TWO ARE SHOWN)
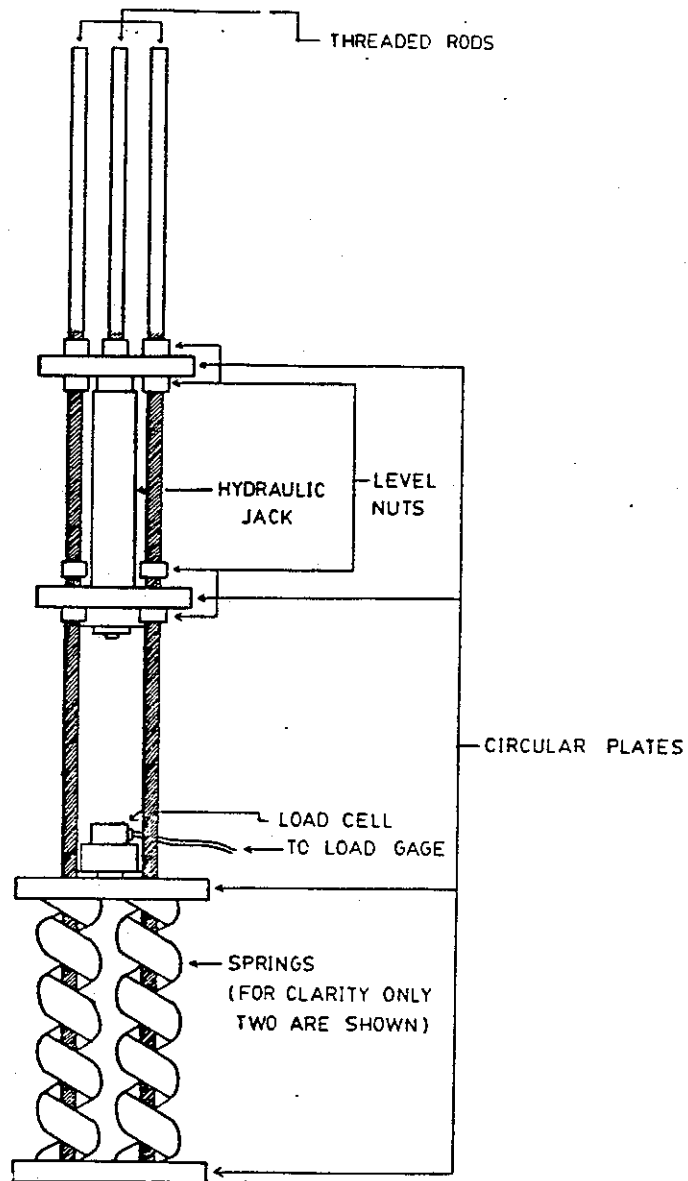
FIGURE 4

SCHEMATIC OF TESTING APPARATUS FOR THE UNIAXIAL

COMPRESSIVE CREEP TEST

14

4.0 THEORETICAL BACKGROUND

4.1 SLOW CRACK GROWTH IN TENSION

In most brittle materials, specifically in silicates and their
glasses, time dependent crack growth under sustained loading
is thought to involve chemical reactions that depend on the
applied stress level. The process of chemically controlled
crack growth in the presence of mechanical stress is called
stress corrosion cracking. In earlier experiments (Charles,
1959), it has been suggested that water corrodes glass
surfaces by interrupting the strong silicon-oxygen bond,
replacing it with the weaker silicon-hydroxyl bond. In the
reaction, the loosely bound alkali ions of the silicate
networks are thought to act as catalysts.

In the stress corrosion of silicates, several mechanisms may
act simultaneously to produce strain through crack growth.
The most obvious mechanisms are, the transport of reagents to
the reaction site, the chemical reaction itself, and the
fracture of corroded bonds after the reaction has taken place.
In multimineral media, such as rocks, each mineral constituent
and the boundaries between them are potential reaction sites.
Each site may have its own operating crack growth mechanism.
Except in those cases where a single mechanism clearly
dominates the deformation process, stress corrosion cracking

15

in rocks is a very complex process.

It has been shown that crack propagation under tensile
loading, due to time dependent stress corrosion, can be
described by the relationship between stress intensity and
crack velocity for almost all materials (Wiederhorn, 1967).
Stress intensity is a measure of the magnitude of stress
occurring at the crack tip in an elastic solid and is a
function of the applied stress, crack size and geometry of the
medium containing the crack. It is represented by the
equation,

$$K = Y\sigma a^{1/2} \qquad [1]$$

where K is the stress intensity factor, σ is the applied
stress (normal to the crack), Y is the geometry factor, and a
is equal to the crack length.

There are up to three regions of crack growth as stress
intensity varies from K_0, the stress corrosion limit, to K_{IC},
the critical stress intensity. All three regions may be
represented on a plot of stress intensity versus crack
velocity, as shown on Figure 5. At low stress intensity,
region I, the rate of chemical reaction near the crack tip
controls the rate of crack growth. At intermediate stress
intensity, region II, the transport of corrosive agents to the

16
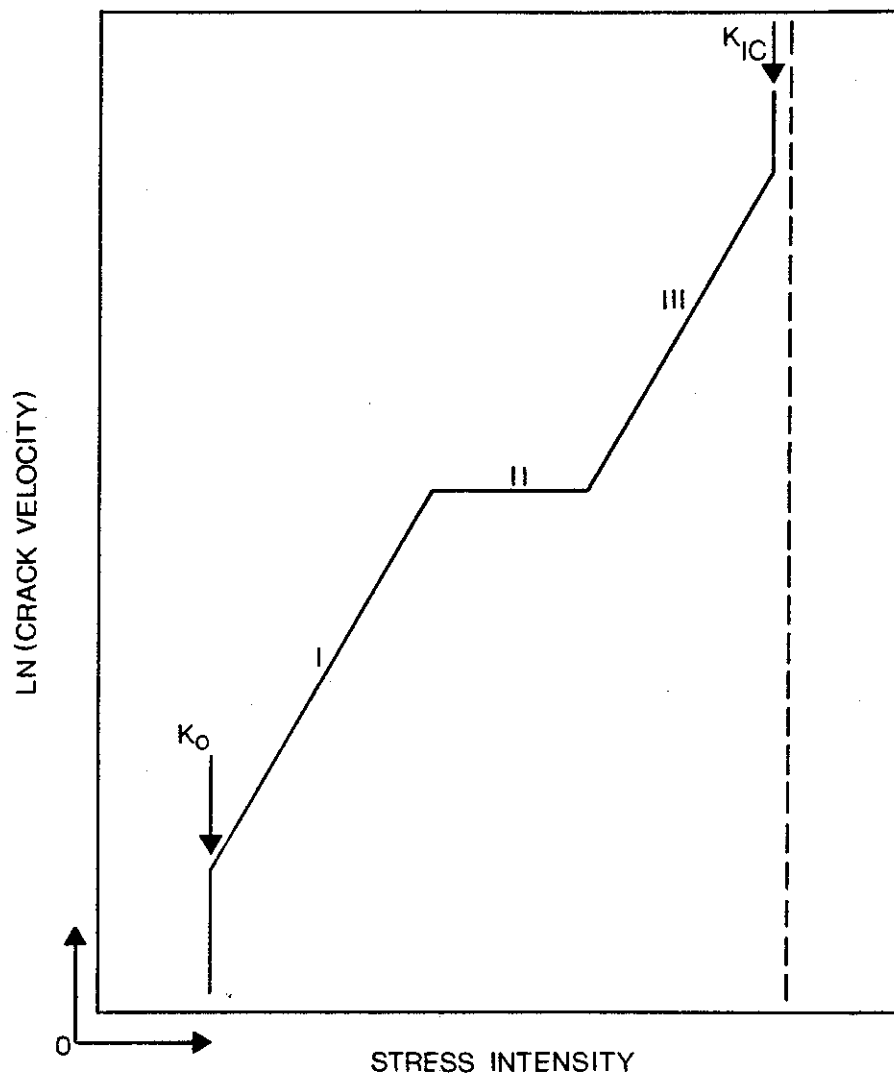
FIGURE 5

THE VARIATION OF CRACK VELOCITY WITH STRESS INTENSITY

FOR A MATERIAL SUBJECTED TO A

STRESS CORROSIVE ENVIRONMENT IN TENSION

17

crack tip controls the rate. At high stress intensity, region
III, a transition occurs from slow stress corrosive crack
growth to rapid unstable mechanical failure (Evans, 1972).

The extent of the three regions varies with each material
tested as well as with the environment the material is
subjected to. However, for most materials the duration of
region I is usually the longest (Anderson, 1977). The crack
velocity for region I is represented by the equation,

$$da/dt = AK^n$$ [2]

where da/dt is the velocity of crack propagation, A and n are
constants, and K is the stress intensity factor at that
velocity. The value of n, is known as the stress corrosion
factor and is dependent on the corrosive environment.

A number of test techniques have been used previously to
obtain values for both stress intensity and crack velocity at
constant load. For transparent materials it is possible to
follow the crack optically, however for opaque materials such
as rock, where the crack cannot be followed visually, the
crack growth rate is usually monitored through a displacement
gauge. The displacement gauge evaluates the crack opening
displacement which is converted into stress intensity or crack
velocity through a compliance calibration (Williams and

18

Nelson, 1970). Compliance is defined as displacement/applied load (y/P), Figure 2.

The double torsion test, which is one of the test procedures used in this study, simplifies the above experimental procedure for both opaque and transparent materials. The primary advantage of the test is the elimination of displacement or optical measurements which are normally required to monitor crack length. Crack growth in the double torsion test is monitored as a function of time through either load or displacement relaxation. Using this technique, stress intensity is no longer dependent on crack length. A discussion on obtaining stress intensity and crack velocity values using the double torsion test is given in the following sections.

4.1.1 THE STRESS INTENSITY FACTOR IN THE DOUBLE TORSION TEST

The double torsion specimen can be considered as two elastic torsion bars, each having a rectangular cross section, loaded as shown on Figure 2, to a load of P/2. It has been shown (Kies and Clark, 1969), that for small deflections, y, and for bars where the width is much greater than specimen thickness, the torsional strain, θ, can be represented by the following equation,

$$\theta = \frac{y}{W_m} = \frac{6Ta}{Wd^3G} \qquad\qquad [3]$$

where T is the torsional moment ($P/2*W_m$), $P/2$ is the total
load applied to one bar, G is the shear modulus of the
material, a is the crack length, d is the bar thickness, $W/2$
is the bar width and W_m is the width of the moment arm.
Equation [3] can then be rearranged to give,

$$\frac{y}{P} = \frac{3W_m^2a}{Wd^3G} = C \qquad\qquad [4]$$

where C is the elastic compliance.

The strain energy release rate for crack extension, g, is
related to the specimen compliance by the following equation,

$$g = \frac{P^2}{2d}(dC/da) \qquad\qquad [5]$$

For a double torsion specimen in which deflections beyond the
crack are negligible, the strain energy release rate can be
obtained by differentiating equation [4] with respect to a and
substituting in equation [5]. This gives,

$$g = \frac{3P^2W_m^2}{2Wd^4G} \qquad\qquad [6]$$

The stress intensity, K, is related to the strain energy
release rate, g, by the following equation,

20

$$K = [2G(1 + \tau)g]^{1/2} \qquad\qquad [7]$$

where τ is Poissons ratio, so that,

$$K = PW_m[3(1 + \tau)/Wd^4]^{1/2} \qquad\qquad [8]$$

The stress intensity factor is thus a function of the applied load, specimen dimensions and Poisson's ratio only and is independent of the crack length.

4.1.2 CRACK VELOCITY

The crack growth rate is obtained using the specimen compliance relationship. The compliance relationship for the double torsion specimen is represented by the equation,

$$\frac{y}{P} = (Ba + D) \qquad\qquad [9]$$

where B is the slope of the curve and D is the intercept. Differentiating equation [9] as a function of time yields the crack velocity, da/dt, plus two easily measured experimental parameters, dP/dt, the rate of change in load and dy/dt, the rate of change in displacement as represented by the equation,

$$da/dt = \frac{dy/dt - (Ba + D)dP/dt}{PB} \qquad\qquad [10]$$

The crack velocity is determined by solving the above equation using the double torsion test under an imposed condition of either constant load or constant displacement.

In the case of constant load, the specimen is loaded at a constant displacement rate until the desired load is reached. The load is then held constant, so that $dP/dt = 0$, and equation [10] reduces to,

$$da/dt = \frac{dy/dt}{PB} \qquad [11]$$

Values for crack velocity are obtained by monitoring the displacement on a continuous basis as a function of time.

For the case of constant displacement, which is the technique used in this study, the specimen is rapidly loaded to a pre-selected load and the cross-head displacement held constant, so that $dy/dt = 0$ and equation [10] reduces to,

$$da/dt = \frac{-(Ba + D)dP/dt}{PB} \qquad [12]$$

At constant displacement,

$$P(Ba + D) = P_0(Ba_0 + D) \qquad [13]$$

where a_0 and P_0 are simultaneous measurements of the crack

22

length and load at either the start or finish of the
relaxation test (Evans, 1972). Substituting for a in equation
[12] gives,

$$da/dt = -\frac{P_o}{P^2}(a_o + D/B)dP/dt \qquad [14]$$

For large a_o, D/B is negligible and equation [14] reduces to,

$$da/dt = \frac{-a_o P_o}{P^2} (dP/dt) \qquad [15]$$

As the crack propagates the load decays and the crack velocity
is obtained from the rate of load relaxation. Load relaxation
is monitored by recording the change in load with time. An
assumption necessary for the use of equation [15] is that
there are no extraneous force relaxations. In other words,
the contribution to dP/dt must come only from crack
propagation with minimal additions from plastic flow and time
dependent distortion of the loading apparatus.

The constant displacement test method was selected, because it
requires monitoring of the load only, yields continuous crack
velocity data directly from the rate of load relaxation and
allows crack velocity to be monitored over several orders of
magnitude.

4.2 SLOW CRACK GROWTH IN COMPRESSION

In compressive loading, crack propagation due to time
dependent stress corrosion can be examined using the
relationship between the crack volume strain and crack volume
strain rate during steady state creep. The stress dependence
of this creep rate can be expressed in a power function
similar in form to that used for crack velocity (McClintock
and Argon, 1966). It is represented by the equation,

$$\dot{\epsilon} = L\sigma^m \qquad [16]$$

where $\dot{\epsilon}$ is the strain rate, σ is the applied stress, and L and
m are constants.

The strain rate power function may also be used for time to
failure predictions providing that the time spent in steady
state creep far outweighs the time spent in primary and
tertiary creep and that the total accumulated strain is a
material constant. If these conditions are met, then the
critical crack volume strain ϵ_{cc}, which is a strain quantity
equal to the total amount of crack volume strain accumulated
before the specimen fails, can be represented by,

$$\epsilon_{cc} = \dot{\epsilon}t \qquad [17]$$

where t is the time to failure for that material (Tetelman and
McEvily, 1967).

To obtain values for the crack volume strain and the crack
volume strain rate, incrementally loaded creep tests are
conducted and the corresponding axial and lateral strains
occurring in the stressed specimen are recorded. These
strains represent the specimen deformation and are easily
translated into a crack volume strain and a strain rate
(Lajtai and Bielus, 1986). Crack volume strains are monitored
until a secondary state creep rate is established at which
point the test is terminated. This rate is determined using
moving linear regression analysis. All three stages of creep
can be obtained if loading is sustained, however, it is more
desirable to obtain several creep rates from each specimen
using incremental loads. During the final loading cycle the
specimen is allowed to enter tertiary creep and eventually
fail. A discussion of crack volume strain and the crack
volume strain rate is given in the following sections.

4.2.1 CRACK VOLUME STRAIN

Derivation of the crack volume strain is based on the
difference between the measured volume strain and the volume
strain due to elastic deformation of the specimen. It is
represented by the equation,

$$\epsilon_c = \frac{(V - V_o)}{V_o} - \frac{(V_e - V_o)}{V_o} \qquad [18]$$

where ϵ_c is the crack volume strain, V is the volume of the specimen at time t under constant uniaxial compressive stress, Ve is the volume the specimen would have at time t under stress if there were no cracks and the specimen deformed elastically, and V_o is the initial no-stress volume of the specimen.

The first term of equation [18] may be computed using the average axial strain, ϵ_A and the average lateral strain, ϵ_L as represented by the equation,

$$\frac{V - V_o}{V_o} = \epsilon_A + 2\epsilon_L \qquad [19]$$

The average axial and lateral strains are calculated using the three axial and three lateral strain gauge values recorded during testing. In contrast to normal rock mechanics practice, compressive stress and strain are considered here to be negative and tensile stress and strain positive. The above expression is therefore negative except at high stresses, close to failure.

Assuming the rock properties to be isotropic, the remaining term of equation [18], which is constant at a constant stress, can be solved using the equation,

$$\frac{V_e - V_o}{V_o} = \frac{\sigma}{E}(2\tau - 1) \qquad [20]$$

where σ is the stress level and E and τ are the isotropic

elastic modulus and Poissons ratio, respectively. The latter

two values can be obtained from the initial or straight line

portion of the stress-strain curve prior to crack initiation.

Following the sign convention stated above, the elastic volume

change is always a negative quantity. The purpose of

departing from the standard rock mechanics sign convention was

to avoid having a negative crack volume.

4.2.2 CRACK VOLUME STRAIN RATE

The crack volume strain rate is based on the time derivative

of equation [18], the crack volume strain. This is simply the

slope of the curve representing crack volume versus time for a

constant applied uniaxial compressive stress. It is

represented by the equation,

$$\dot{\epsilon} = d\epsilon_c/dt \qquad [21]$$

where $\dot{\epsilon}$ is the crack volume strain rate, ϵ_c is the crack

volume strain and t is the time of the crack volume strain.

The purpose of calculating the crack volume strain rate is to

develop a relationship between the applied stress and the

proportion of crack growth which will occur at that particular

stress level. From this relationship one can then determine a potential time to failure value and ultimately a safe working stress level.

The volumetric strain rate can be related to a stress level using the power function shown in equation [16]. Combining this function with equation [17], the time to failure, one can develop a simple relationship between time and stress. This relationship is represented by the equation,

$$t = \epsilon_{cc}/L\sigma^m \qquad [22]$$

This equation enables one to calculate the time to failure given a particular stress level.

5.0 TEST RESULTS AND DISCUSSION

5.1 MEASUREMENT OF CRACK VELOCITY

Crack velocity and stress intensity measurements have been made using the double torsion test. A total of 16 tests were completed in which the test specimens were subjected to one of three controlled environments. The first, involving seven tests, was a dry environment, where the specimens were tested at room temperature and room humidity, approximately 25 degrees celsius and 25 percent relative humidity respectively. The second, involving five tests, was a wet environment, where the specimens were tested at room temperature, 25 degrees celsius, but completely submerged in water. The third, involving four tests, was a hot wet environment, where the specimens were completely submerged in water but at a temperature of 90 degrees celsius.

For each test, the specimen was placed within the testing apparatus and subjected to a pre-selected load equal to 69 to 89 percent of the specimens critical stress intensity factor. The critical stress intensity factor is the maximum stress intensity attainable prior to failure. This value was calculated for each specimen by eventually failing it through rapid load up. Once the pre-selected load had been applied, the cross-head displacement was held constant and the load

29

allowed to relax as crack propagation occurred. The load

relaxation was monitored with time and values for stress

intensity and crack velocity calculated from the applied load

and relaxation rate at each time interval, respectively. A

double log plot of crack velocity versus stress intensity was

then constructed and the data points fitted to a straight line

curve using a least squares fit. The slope and intercept of

the least squares line were calculated, where the slope is

equivalent to the stress corrosion factor n and the intercept

equal to the constant A as represented in equation [2].

The results of these tests are shown on Figures 6 to 8 for the

dry, wet and hot wet environments respectively. Each figure

includes the plots of the individual tests as well as a

summary table of the initial stress intensity factors to which

each specimen was subjected, (K_i) and the corresponding stress

corrosion factor, (n) for each curve. The average stress

corrosion factor for each environment is also shown with

values of 96 for dry, 54 for wet and 25 for hot wet. The

median values are likely more representative of the true

values with stress corrosion factors for the three

environments of 91, 52 and 25 respectively.

In viewing Figures 6 to 8, it can be seen that within any one

environment, the stress applied to the specimen has no effect

on the resulting value of the stress corrosion factor. The

The figure plots LN(VELOCITY, m/s) on the left axis (from -7 to -17) versus LN(STRESS INTENSITY K, MPa·m$^{1/2}$) on the bottom axis (from 0.60 to 1.00). The top axis shows STRESS INTENSITY K, MPa·m$^{1/2}$ (2.00, 2.25, 2.50, 2.75). The right axis shows VELOCITY, m/s (10^{-4}, 10^{-5}, 10^{-6}, 10^{-7}) with "Start of test" at top and "End of test" at bottom.

DRY , 25 °C

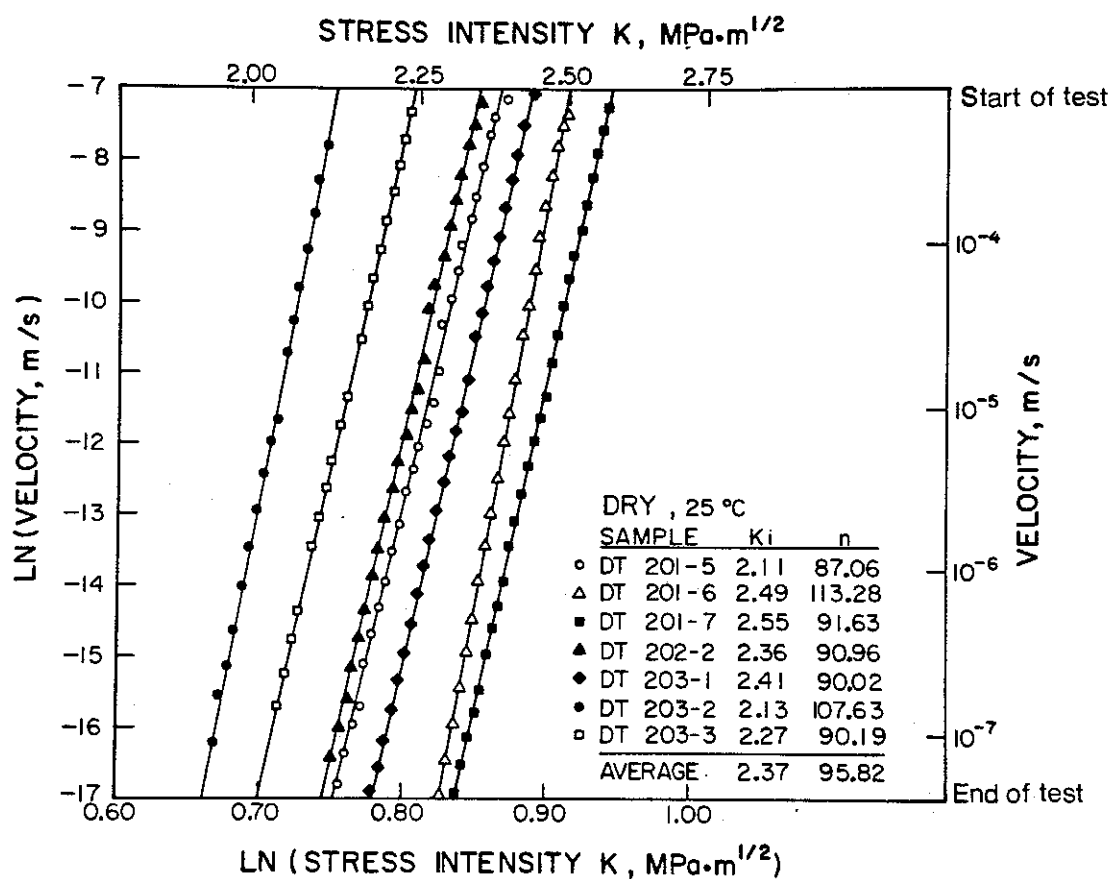| SAMPLE		K_i	n
○	DT 201-5	2.11	87.06
△	DT 201-6	2.49	113.28
▪	DT 201-7	2.55	91.63
▲	DT 202-2	2.36	90.96
◆	DT 203-1	2.41	90.02
●	DT 203-2	2.13	107.63
▫	DT 203-3	2.27	90.19
	AVERAGE	2.37	95.82

FIGURE 6

CRACK VELOCITY VERSUS STRESS INTENSITY IN THE DOUBLE

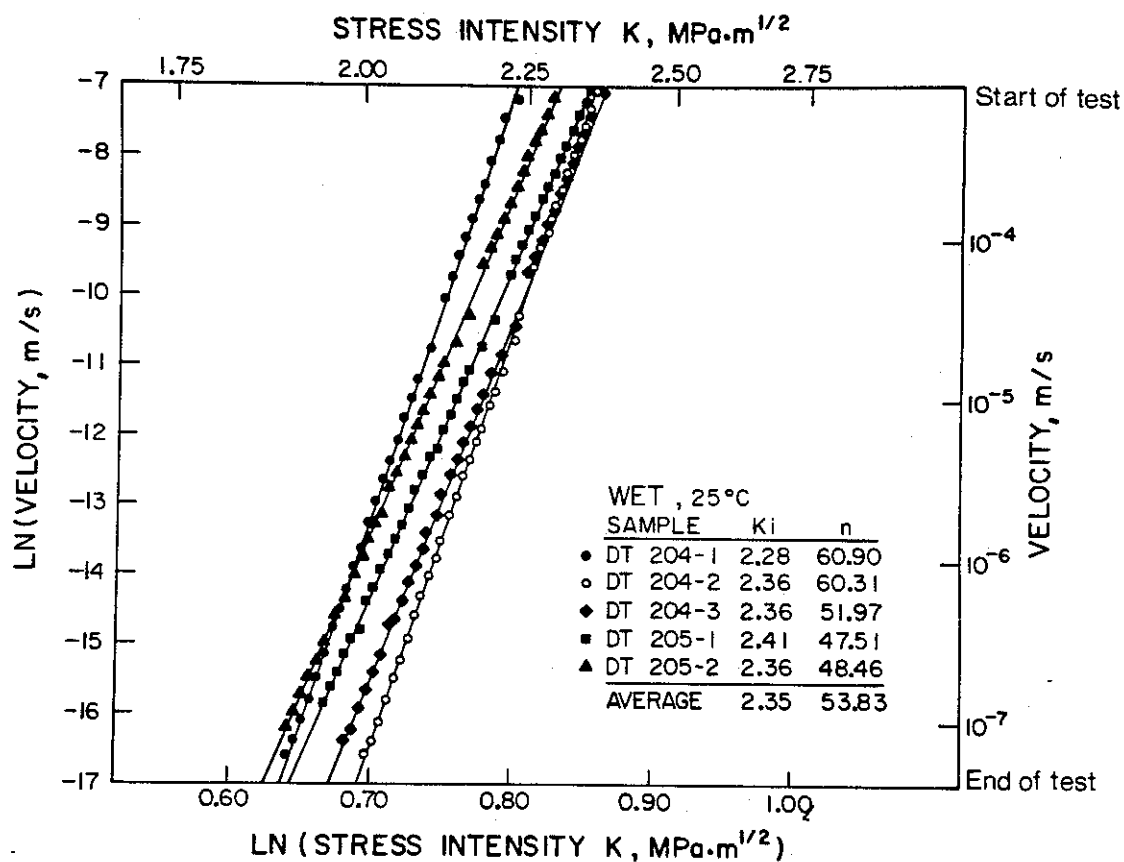TORSION TEST FOR THE DRY ENVIRONMENT (ALL TESTS)

31

FIGURE 7

CRACK VELOCITY VERSUS STRESS INTENSITY IN THE DOUBLE

TORSION TEST FOR THE WET ENVIRONMENT (ALL TESTS)
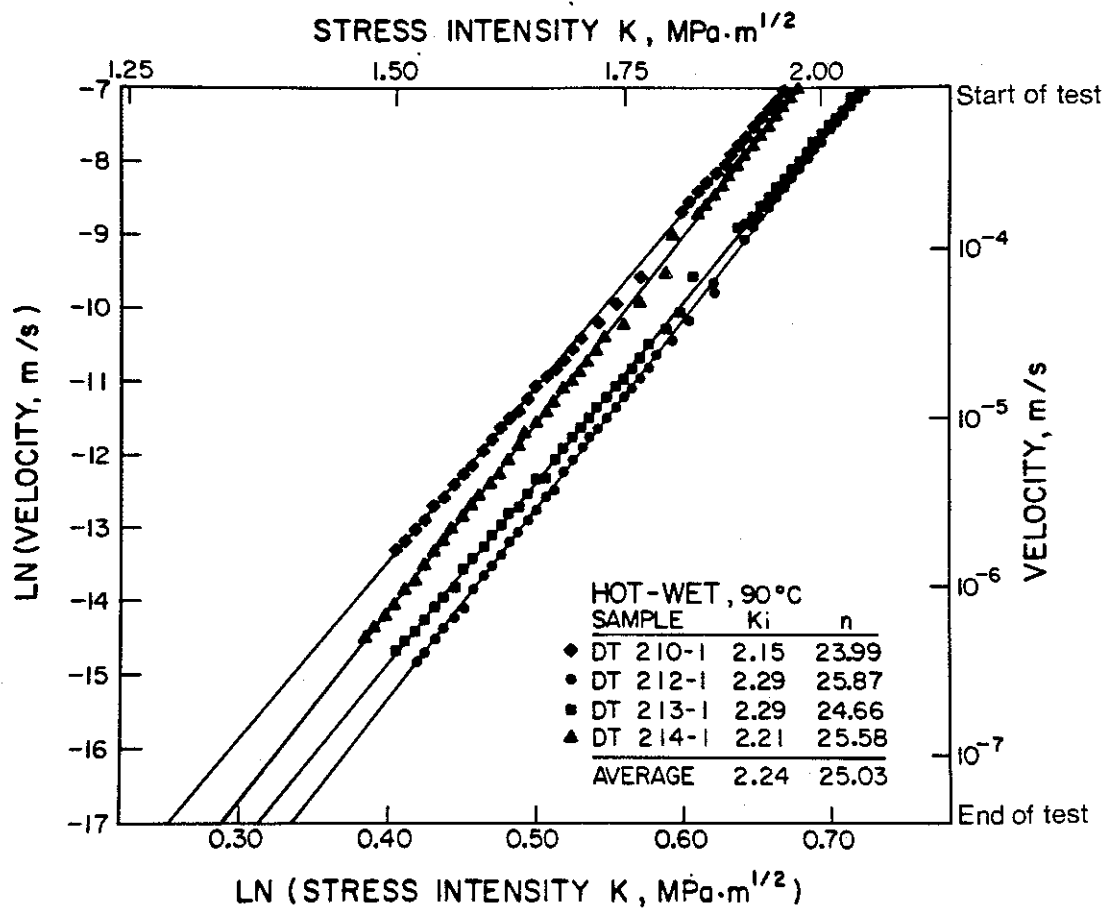
FIGURE 8

CRACK VELOCITY VERSUS STRESS INTENSITY IN THE DOUBLE

TORSION TEST FOR THE HOT WET ENVIRONMENT (ALL TESTS)

only effect of changing the stress level is to cause a

parallel shift of the straight line curve to either the right

or left at respectively higher and lower stress levels.

Although the stress level has no effect on the stress

corrosion factor, the environmental conditions do. A decrease

in the stress corrosion factor of 45 percent is observed

between the dry (91) and wet (52) environments and a decrease

of 72 percent between the dry (91) and hot wet (25)

environments. The lower stress corrosion factor represents a

greater material sensitivity to stress corrosion cracking.

The sensitivity of the stress corrosion factor to

environmental change, especially dry to wet, is well

documented. Table 2 is a summary of stress corrosion values

for a variety of materials tested in the dry and/or wet

environment under tensile loading. As presented in Table 2

most materials, like LDB Granite, have a stress corrosion

factor in the order of 10 to 80. As well, most materials show

a decrease in the stress corrosion factor when conditions

change from room temperature and humidity (dry environment) to

room temperature and 100 percent humidity (wet environment).

A direct comparison of the effects of the three environments

is shown on Figures 9 and 10, in which three identical

specimens were initially loaded to approximately the same

stress intensity level but subjected to different

TABLE 2

STRESS CORROSION FACTORS

FOR

MATERIALS UNDER TENSILE LOADING

MATERIAL	DRY	WET	REFERENCE
SODA-LIME SILICATE GLASS	21	14	Wiederhorn, 1970
ALUMINO SILICATE GLASS		25	Wiederhorn, 1970
SILICA GLASS		42	Wiederhorn, 1970
BOROSILICATE GLASS		24	Wiederhorn, 1970
LITHIUM ALUMINOSILICATE	43		Wiederhorn, 1978
MAGNESIUM ALUMINOSILICATE	82		Wiederhorn, 1978
TRANSDUCER CERAMIC PZT		50	Bruce et al, 1978
PORCELAIN		40-60	Matsui et al, 1978
ANDESITE	31	9	Toshihiko, 1980
BASALT	36	32	Toshihiko, 1980
ANORTHOSITE	58	17	Denesiuk, 1983
LDB GRANITE	91	52	This Study

environmental conditions. Figure 9 is a plot of the stress

intensity versus displacement (loading curve) and the stress

intensity versus time (load relaxation curve). In this

figure, K_u represents the stress intensity factor when crack

arrest occurred, that is the point at which load relaxation

became asymptotic. The times shown on the right hand side

indicate when this occurred. An exception to this is the hot

wet test, where the time indicated represents when the

specimen failed. Figure 10 is a plot of crack velocity versus

stress intensity, interpreted on the basis of equation [2],

for the three environments tested. The power function

equation of each curve is also shown with respective stress

corrosion factors of 90, 60 and 26.

Figures 9 and 10 both show the effect of time dependence on

stress corrosion cracking. During rapid load up, time

dependent cracking is not a factor and therefore the loading

curves and the initial relaxations show almost no

environmental influence. During load relaxation, when time

dependent stress corrosion cracking can occur, the

environmental influence is observed by an increase in the load

decay.

The environmental influence is most evident on Figure 10 where

the three curves appear to diverge from a common point of

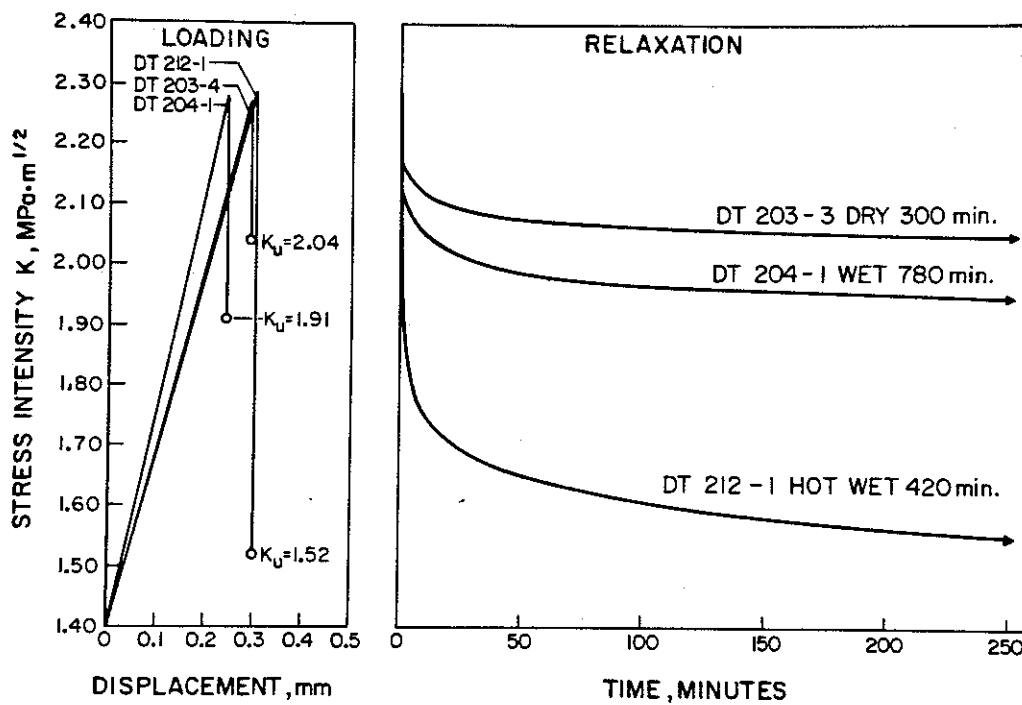intersection at high stress intensity and crack velocity. At

FIGURE 9

LOADING AND RELAXATION CURVES IN THE DOUBLE

TORSION TEST FOR THE DRY, WET AND HOT WET

ENVIRONMENTS USING THREE SIMILAR SPECIMENS

FIGURE 10

CRACK VELOCITY VERSUS STRESS INTENSITY IN THE
DOUBLE TORSION TEST FOR THE DRY, WET AND HOT WET
ENVIRONMENTS USING THREE SIMILAR SPECIMENS

38

the intersection point crack propagation is so quick that
there is insufficient time for the environment to react with
the crack tip. As stress intensity and crack velocity
decrease then time dependent stress corrosion becomes a
factor. More time is available for the environment to react
with the crack tip and therefore divergence of the curves is
observed.

Two other tests were completed to show how environmental
conditions affect stress corrosion cracking within the same
specimen. These tests were designed to avoid specimen to
specimen variation in material properties. In the first test,
a specimen was subjected to two cycles of loading, with the
cycles separated by full unloading. During the first cycle no
water was used and during the second cycle, the same specimen
was flooded with water at room temperature. A plot of the
stress intensity and crack velocity values for both cycles are
shown on Figure 11. The derived equations for the two curves
are also shown. The resulting values of stress corrosion, 56
for the dry and 41 for the wet environment, are slightly lower
than typically obtained for dry and wet conditions, however
the same environmental and time dependent effects are still
observed.

In the second test, a specimen was loaded in a dry condition
but after one minute was flooded with water while still

STRESS INTENSITY, MPa·m$^{1/2}$

LDB Granite
Slow Crack Velocity
Double Torsion
DT-259

$V = 7.97 \times 10^{-17} K^{41}$

$V = 4.29 \times 10^{-22} K^{56}$

ln (Velocity, m/s)

VELOCITY, m/s

WET
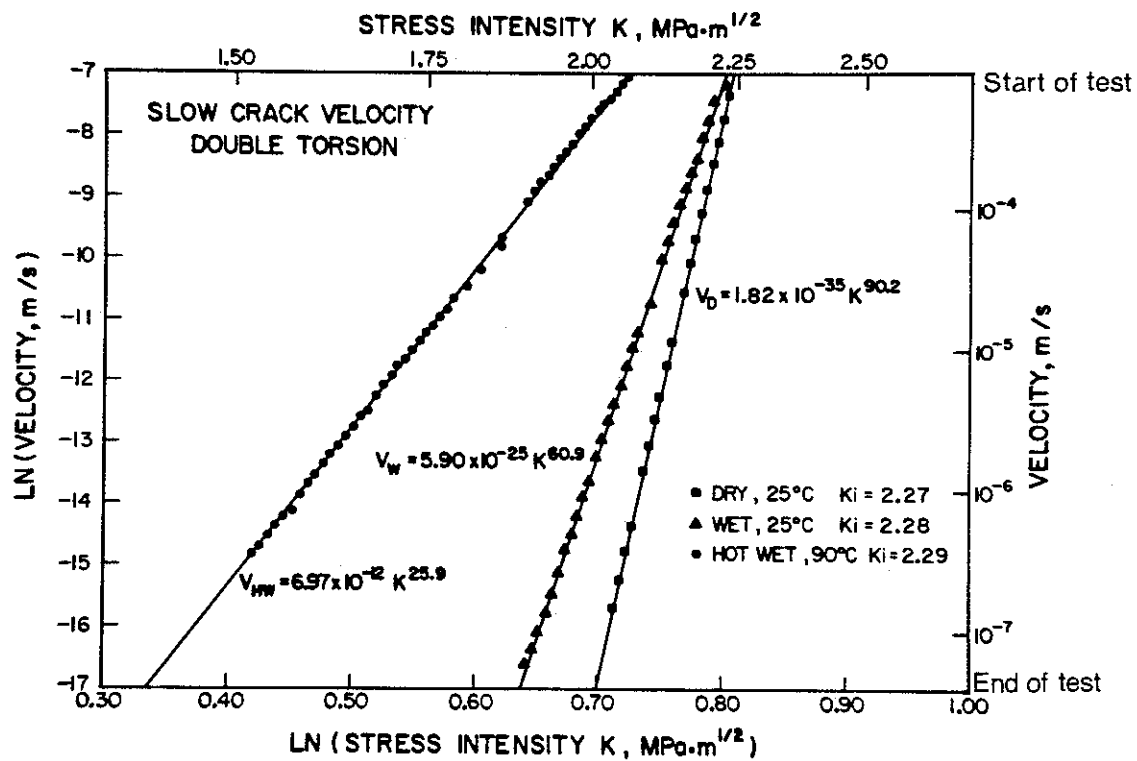
DRY

Start of test

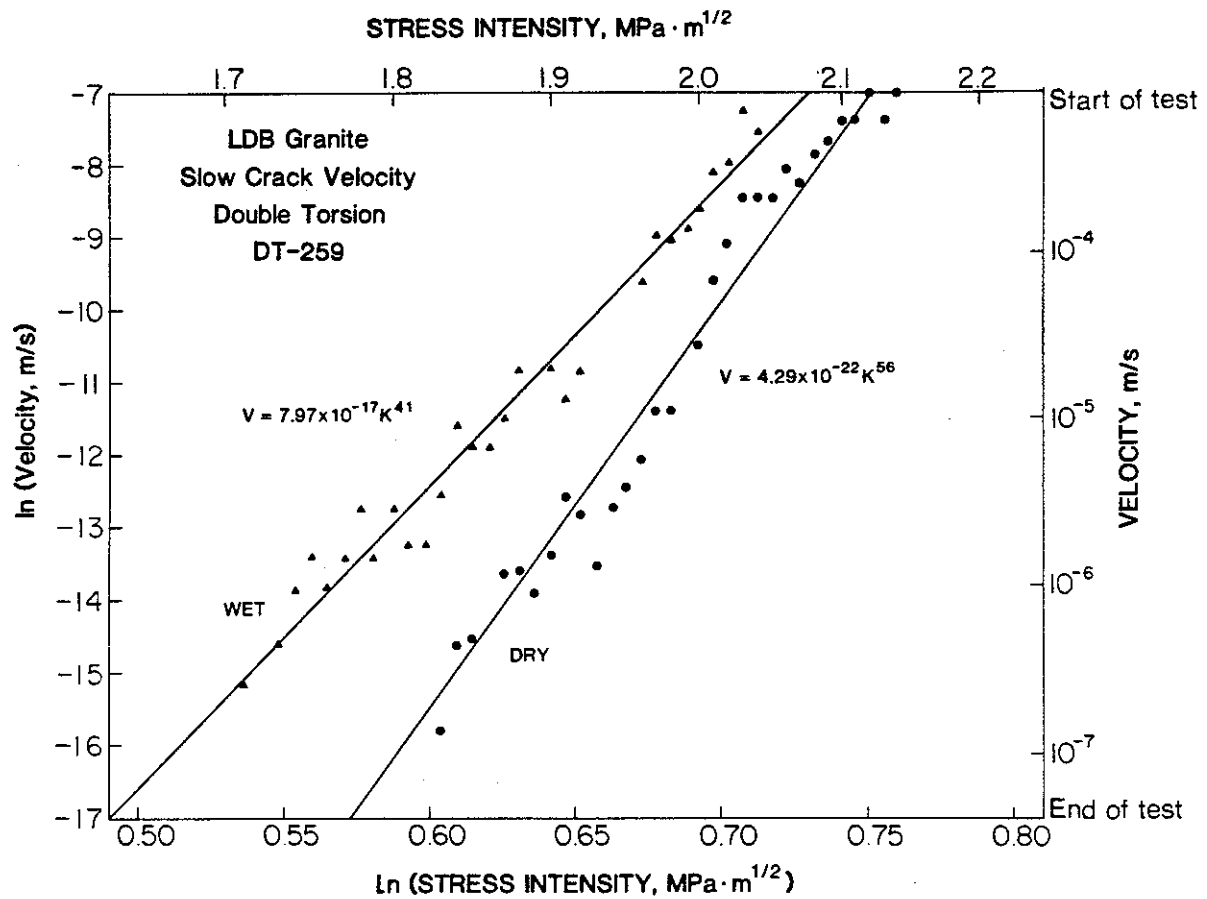End of test

ln (STRESS INTENSITY, MPa·m$^{1/2}$)

FIGURE 11

CRACK VELOCITY VERSUS STRESS INTENSITY IN THE

DOUBLE TORSION TEST FOR THE DRY AND WET ENVIRONMENTS

USING THE SAME SPECIMEN FIRST LOADED DRY THEN LOADED WET

loaded. A plot of crack velocity versus stress intensity is shown on Figure 12. Equations for the dry and wet portions of the curve were derived and are also shown on the figure. Once again the stress corrosion factors are lower than normal, however the same environmental effect and time dependence is observed. With the addition of water a velocity change of over one order of magnitude was achieved almost immediately.

To further illustrate the limit of time dependence at high stress levels, fracture toughness determinations were completed. Fracture toughness (critical stress intensity factor) is the maximum stress intensity factor attainable through rapid load up. Figure 13 is a plot of fracture toughness versus cumulative probability (Weibull Distribution) for the dry and wet environments. As can be seen by the plot, where the loading rate is high there is almost no difference between the two distributions indicating very little time dependence and consequently very little environmental influence.

5.2 MEASUREMENT OF CRACK VOLUME STRAIN

The axial and lateral strain parameters needed to define the crack volume strain and its rate were obtained from uniaxial compressive creep tests. A total of seventeen tests were completed on specimens subjected to either dry or wet
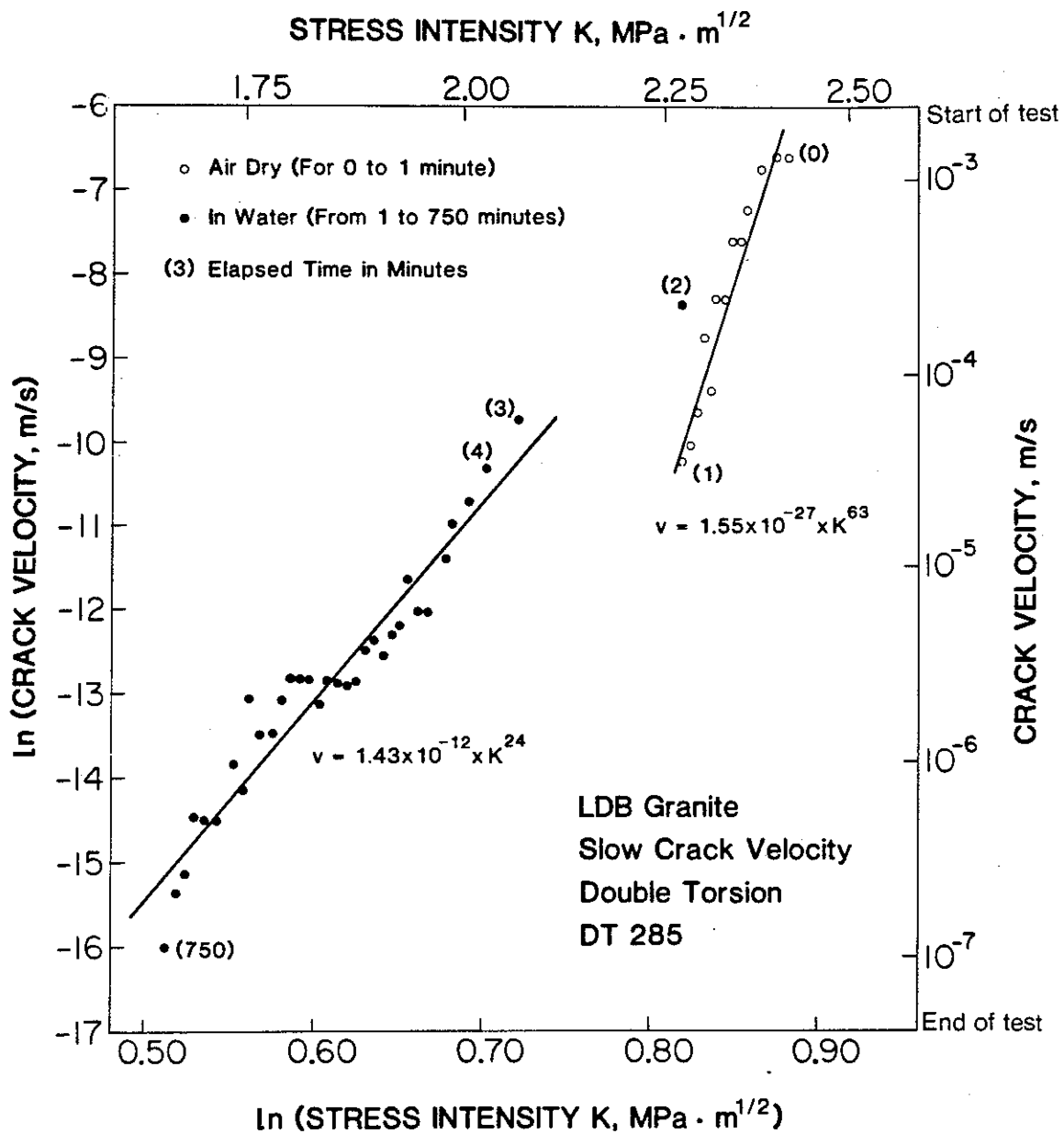
FIGURE 12

CRACK VELOCITY VERSUS STRESS INTENSITY IN THE DOUBLE
TORSION TEST FOR THE DRY AND WET ENVIRONMENTS USING
THE SAME SPECIMEN LOADED DRY THEN FLOODED WITH WATER
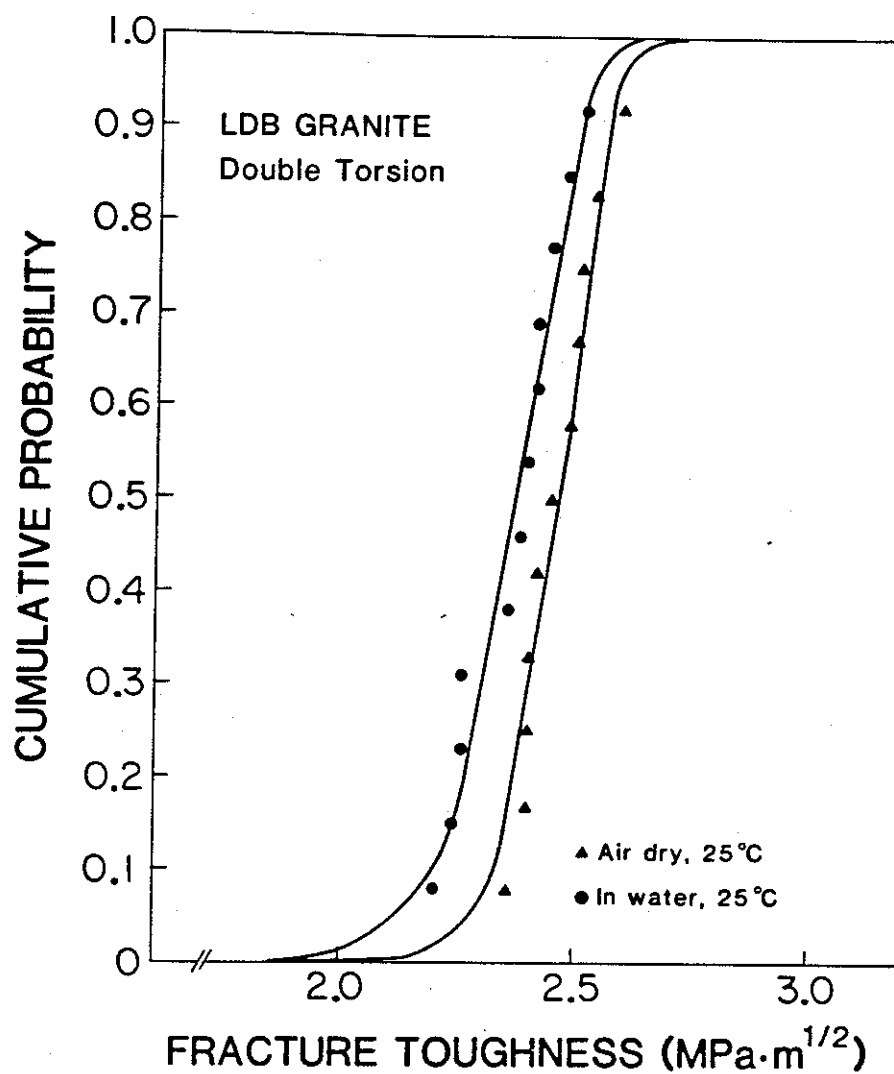
FIGURE 13

THE CUMULATIVE PROBABILITY DISTRIBUTION OF

FRACTURE TOUGHNESS IN THE DOUBLE TORSION TEST

FOR THE DRY AND WET ENVIRONMENTS

environments. A hot wet environment was not analyzed due to difficulties of maintaining electronic control at elevated temperatures. A number of additional tests were also completed but were proven invalid as more rigorous computer analysis of the data indicated that the tests were terminated too early as they were still in the primary stage of creep. Primary creep can be very long when the stress is relatively low. For example, test 709-1 at the 117 MPa load had not entered into steady state creep after 16 days of testing. A summary of the test specimens, testing environment, stress level and strain rate is presented in Table 3.

Specimens 519 and 707 were subjected to incremental load creep testing and produced respectively, four and three reliable rate measurements as shown in Table 3. Measured strain rates less than about 10^{-11} s^{-1} are unreliable as the no load drift of the instrumentation is typically between 10^{-12} s^{-1} and 10^{-11} s^{-1}. Specimen 709 produced two usable rate measurements, specimens 706, 710 and 714 only one. Creep curves for specimens 519 and 707 are shown on Figure 14. The strain rate data are plotted on Figure 15.

Figure 14 demonstrates the influence of moisture on time dependent deformation. In the dry series, no steady state creep was observed until 150 MPa. At this load, the rate of 10^{-11} s^{-1} is approximately one fifteenth of the rate of test

TABLE 3

STRESS LEVEL VERSUS CRACK VOLUME STRAIN RATE

| SPECIMEN	ENVIRONMENT	LOAD (MPa)	RATE (s^{-1})
519-1	DRY	102	*
519-2	DRY	125	*
519-3	DRY	150	2.0×10^{-11}
519-4	DRY	175	1.2×10^{-10}
519-5	DRY	190	2.4×10^{-10}
519-6	DRY	200	5.0×10^{-10}
706-4	WET	140	1.4×10^{-10}
707-4	WET	133	5.9×10^{-11}
707-5	WET	140	9.3×10^{-11}
707-7	WET	150	4.5×10^{-10}
708-1	WET	50	*
708-2	WET	75	*
708-3	WET	100	*
709-2	WET	126	3.8×10^{-11}
709-3	WET	136	1.7×10^{-10}
710-1	WET	144	2.3×10^{-10}
714-1	WET	137	8.5×10^{-11}

* No strain rate was measured at these loads.
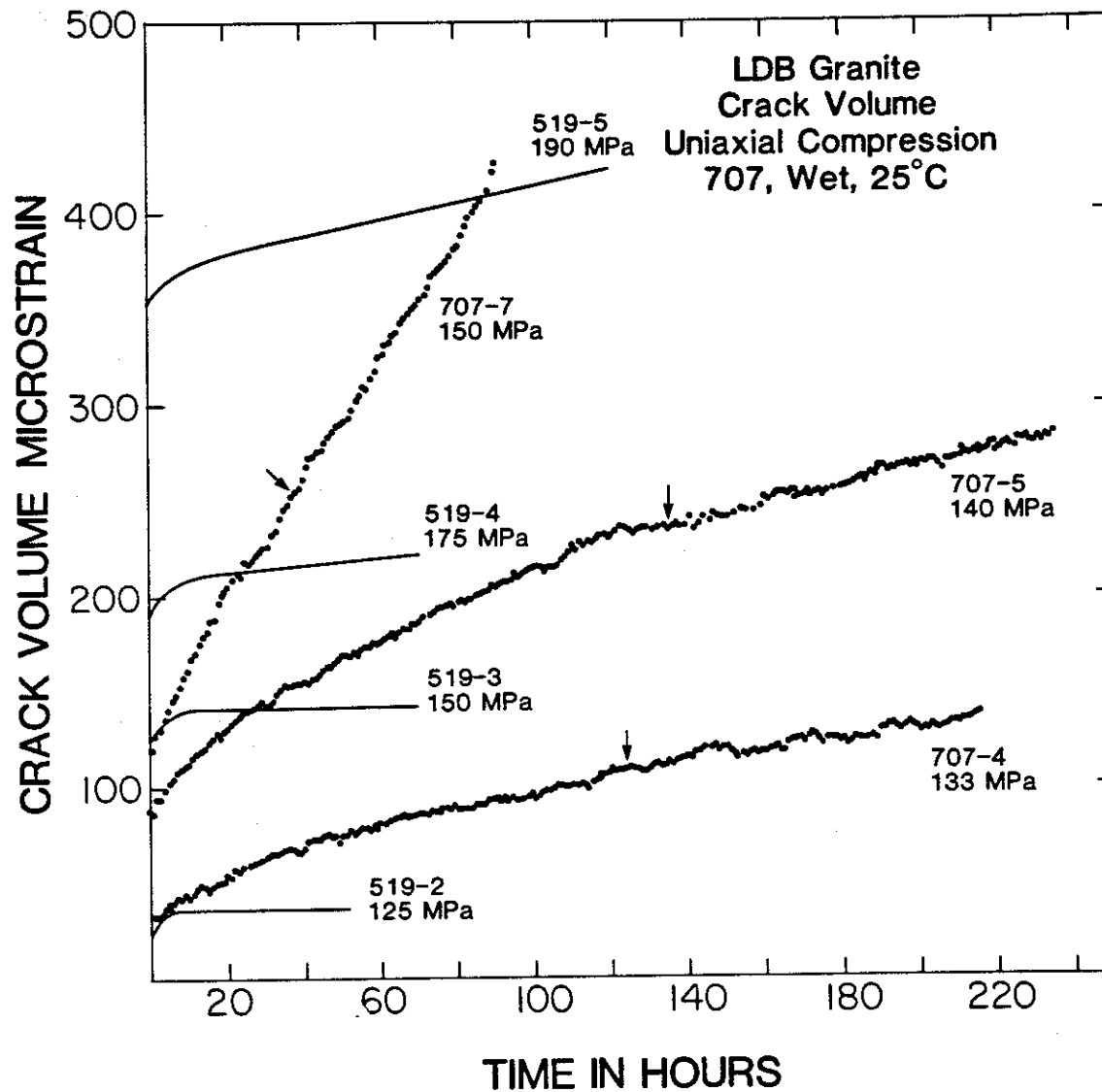
FIGURE 14

CRACK VOLUME VERSUS TIME IN THE UNIAXIAL COMPRESSIVE

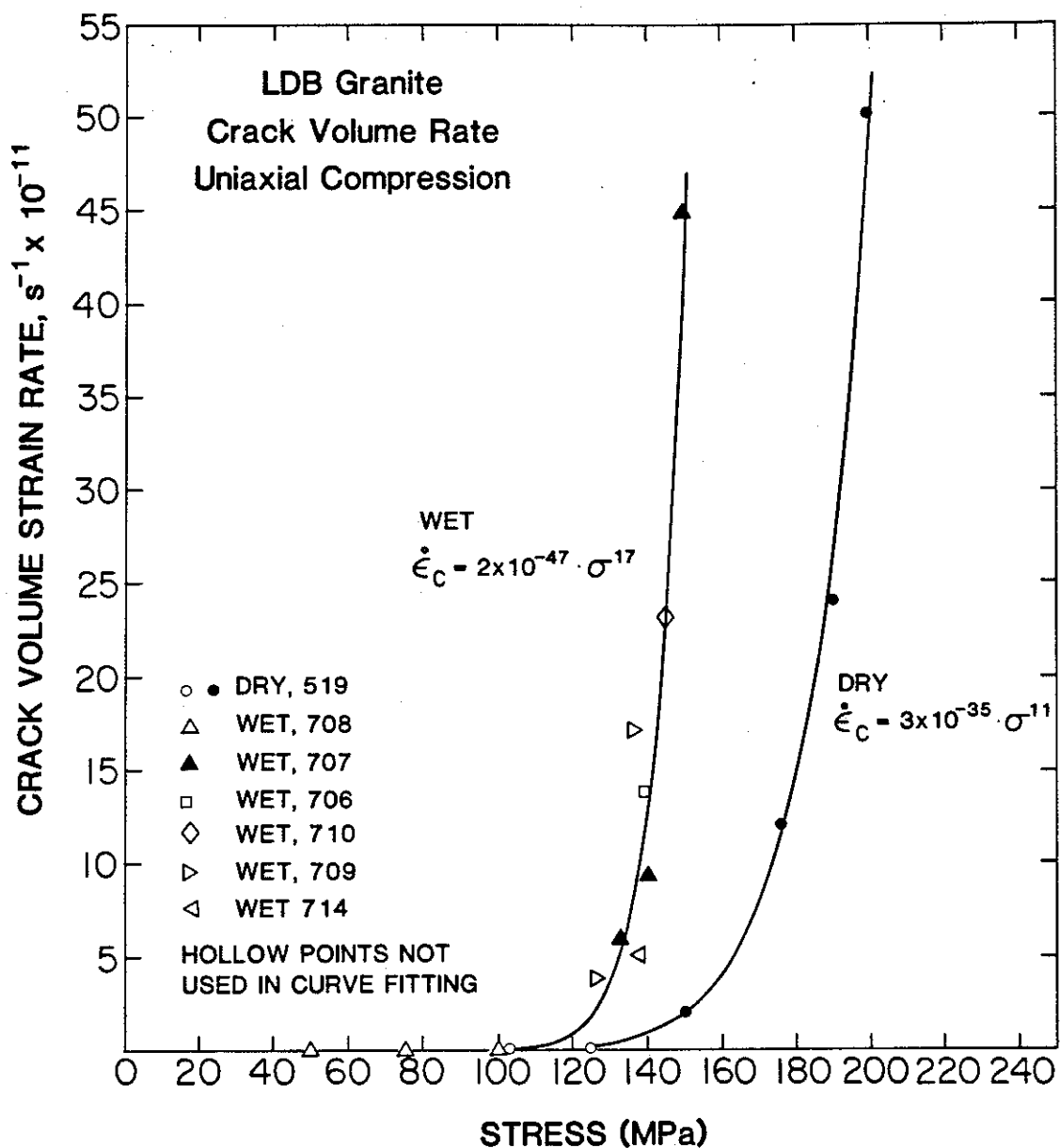CREEP TEST FOR THE DRY AND WET ENVIRONMENTS

46

FIGURE 15

CRACK VOLUME RATE VERSUS STRESS IN THE UNIAXIAL
COMPRESSIVE CREEP TEST FOR THE DRY AND WET ENVIRONMENTS

707-7 conducted at the same load but in a wet environment. The lowest stress at which steady state rate has so far been measured is 126 MPa in the wet environment.

Figure 15 demonstrates the stress dependence of the steady state creep rate for dry and wet environments. The curves have been fitted to a power function (equation 16) similar in form to the one used in the double torsion test. Although the three measurements for 707 and the four measurements for 519 provide only the bare minimum for curve fitting, the power function fits the data quite well with correlation coefficients of 0.99 for the dry and 0.90 for the wet environment. Strain rate measurements plotted from other tests are generally in agreement with the trends established by the above two.

The correlation coefficient for the wet curve was relatively low and therefore a number of other mathematical functions have been fitted to the data as well. Table 4 presents a summary of some of the better correlations obtained from the other functions tested. The exponential function gives a slight improvement in correlation, but it is the hyperbolic functions that fit the three data points of test 707 the best. The hyperbolic functions however, predict measurable creep rates in the 50 to 100 MPa range which is not supported by the data from the creep tests. The power function on the other

48

hand suggests that demonstrating steady state creep rates at axial stresses as low as 120 MPa should be possible. This agrees quite well with the creep test data.

TABLE 4

CURVE CORRELATION COEFFICIENTS

FOR

CRACK VOLUME STRAIN RATE VERSUS STRESS

FUNCTION	COEFFICIENT OF CORRELATION	
	DRY	WET
$Y = AX^B$	0.9934	0.9015
$Y = Ae^{By}$	0.9902	0.9155
$Y = 1/(A + BLnX)$	0.8359	0.9999
$Y = 1/(A + BX)$	0.7972	0.9998
$Y = 1/(A + B/X + C/X^2)$	0.9934	0.0000

5.3 PREDICTING TIME TO FAILURE

Predictions for time to failure at a constant stress (equation 22), can be obtained by integrating the strain rate function (equation 21) between time zero, entry into steady state creep, and the time to failure, time for entry into tertiary creep. To make use of this relationship, the value of ϵ_{cc} must be shown to be a material constant. To date, based on limited test data, this value ranges between 500 and 2000 microstrain. Fortunately, the stress at which failure occurs at time t is not very sensitive to ϵ_{cc}. Expressing equation [22] as a function of σ,

$$\sigma = (\epsilon_{cc}/Lt)^{1/m} \qquad [23]$$

and substituting a typical value of $\epsilon_{cc} = 1000$ microstrain and t = 1000 years, the strength of LDB Granite in the wet environment works out to be 87 MPa. Using 500 and then 2000 microstrain for ϵ_{cc}, the computed stress only moves down and up by 4 MPa, respectively. The 87 MPa strength represents slightly less than 40 percent of the dry mean instantaneous compressive strength of LDB Granite.

The predicted strength of granite after 1000 years of sustained loading depends, of course, on the type of mathematical function selected to represent the crack volume

50

strain rate versus stress relationship. The hyperbolic

function (Table 4), which best fits the wet environment, would

predict zero strength after only a few years of loading. The

exponential function predicts 97 MPa, or 10 MPa higher than

the power function. This represents 43 percent of the dry

instantaneous strength.

The power and the exponential relationships between strain

rate and stress predict strength reduction with time that is

greater than the reduction predicted from short term static

fatigue tests (Lajtai and Schmidtke, 1985). Lajtai and

Schmidtke (1985), estimated on the basis of static fatigue

tests that the 1000 year strength lies in the 120 to 140 MPa

range. The mid point of 130 MPa represents 60 percent of the

instantaneous strength. This is substantially higher than the

40 percent estimated from the present series of creep tests.

The rather large difference between the two values is not

surprising. Static fatigue tests are relatively short

experiments and at the high stresses used, the failure time is

dominated by the time spent in primary and tertiary creep.

The estimate derived from creep tests, on the other hand, is

based on time spent in steady state creep. In longer term

creep tests, involving weeks of testing, time spent in steady

state creep would dominate. When considering the service life

of engineering projects, measured in tens to hundreds of

years, life time estimates based on long term creep tests

(days to weeks) should be more reliable than static fatigue

tests involving tests ranging from seconds to days in

duration.

6.0 MICROSTRUCTURAL AND MINERALOGICAL CONTROL ON CRACK GROWTH

Microstructural and mineralogical control on crack growth has been observed as a function of both tensile and compressive loading. Using the double torsion test, tensile crack growth was observed under an optical microscope both in-situ, as crack propagation occurred and through after test examination of the fractured specimen. Thin sections of the failed specimen were also viewed using transmitted light microscopy. Compressive crack growth was observed using only transmitted light microscopy on thin sections cut from failed and unfailed compressive test specimens.

6.1 CRACK GROWTH IN TENSION

The double torsion test is a useful means of allowing direct visual observation of the cracking process. In monomineralic and fine grained ceramic materials a crack can be seen to advance along the long dimension of the test specimen at velocities that agree with theory. In the multimineral and relatively coarse grained granite, the fracture process is much more complex. A major propagating crack can be seen as expected by theory, however crack growth is intermittent with periods of rapid growth over small distances followed by periods when the main crack front is almost stationary. Discontinuous crack formation ahead of the main crack front is

common and several cracks may propagate at the same time.
Branching from the main crack and coalescence of sub-cracks
with the main crack have both been observed (Borynsky, 1983).
The average measured crack velocity therefore must be regarded
only as a measure of a more complex crack advance process.

The microstructure and mineralogy of LDB Granite has a strong
influence on the crack path (Svab and Lajtai, 1981).
Approximately 15 percent of the crack advance occurs along
grain boundaries with 60 percent along cleavage planes in
microcline, oligoclase and biotite. Microcline and oligoclase
offer the least resistance to propagating cracks. Fracture in
these minerals is generally transgranular, occurs abruptly and
often forms a step like pattern along their cleavage planes.
Biotite, although mineralogically composing the lowest
percentage, exerts the most resistance to transgranular
propagation. Frequently fractures enter biotite grains and
either stop completely or only travel part way through.
Eventually a crack or a multiple of cracks start at the
opposite side and continue to propagate as a single crack.
When a crack enters the biotite grain parallel to cleavage the
fracture pattern is similar to that of microcline and
oligoclase. The remaining 25 percent of the crack advance
involves bulldozing through quartz. This is a complex
fracture process involving multiple cracking which generally
occurs along the grain boundaries of the polycrystalline

quartz grain.

Due to this strong microstructural and mineralogical control over crack propagation the major crack does not follow a straight path. Disregarding secondary fracturing (branching cracks and other cracks not connected with the major crack), the length of the actual fracture path is approximately twice as long as the distance between the starting and end points of the major crack (Ross, 1982). In the double torsion test and in the uniaxial tension test (Lajtai, 1981; Bielus, 1982), the propagating crack seems to take advantage of every weak direction it encounters. Ninety degree turns in the crack path are quite common, when the crack encounters grain boundaries. The proportion of crack branching and cracking not associated with the major crack is quite variable, with ratios of one to two times the major crack length (Borynsky, 1983).

Despite the differences in the pattern of crack advance in ceramics and granite, there are many similarities. Granite shows the same type of sensitivity to stress corrosion cracking and although granite is a polymineral medium, the measured velocity data are no more complex in trend and distribution than data from tests on monomineralic ceramic materials. Furthermore, the effect of moisture is also similar, both showing higher crack velocities in the wet

environment than the dry environment.

6.2 CRACK GROWTH IN COMPRESSION

Although the mechanism of crack advance in the double torsion
test appears to be more complex in granite than in glasses and
ceramics, it is possible to identify a major crack and
calculate the velocity of its advance. Crack growth in
uniaxial compression however, is significantly different
(Lajtai, 1981). Although cracks take advantage of suitably
orientated planes of weakness, such as grain boundaries and
cleavage planes in feldspars, the crack propagation direction
for an individual crack at any moment is usually within 10
degrees of the compression axis.

At lower stress levels most cracks appear to grow in feldspar
grains along suitably oriented cleavage planes. With
increasing stress, the density of cracking also increases as
additional vertical cracks develop parallel to and
independently from each other. As the stress level reaches
the failure point cracking in quartz is the dominant process.
Once failed, crack paths are observed to orientate themselves
towards the direction of the shear plane. This is believed to
be a result of the coalescing effects of transgranular cracks
which produce the shear plane. Around the shear plane it has
also been observed that there is intense multi-track cracking

56

and cataclastic brecciation (Bezys, 1984).

Observations of the mineralogic control on crack growth in
compression suggest that both crack initiation and arrest take
place at quartz and biotite grains. Some cracks upon
approaching a small biotite grain have even been observed to
abruptly change their path to avoid the mineral. These
deflections although significant events are minor in scale and
not different from the pattern already noted in tension. The
feldspars, as in tension, offer little resistance to crack
growth and rapid crack movements through them appear to start
and stop at biotite and quartz concentrations (Lajtai, 1981).
An investigation of mineralogic control on crack initiation
was completed using strain gauges mounted over individual
minerals and noting the corresponding breaking point on the
stress-strain curve for that gauge (Harper, 1985). The
findings were vague, but did indicate that crack initiation
generally occurred at the lower stress levels for those gauges
mounted over feldspars and at higher stress levels for those
mounted over quartz.

7.0 CONCLUSIONS

The double torsion and uniaxial compressive creep tests are an
excellent means of evaluating time dependent stress corrosion
cracking in LDB Granite under tensile and compressive loading,
respectively. Both techniques utilize simple specimen
geometries and testing procedures that allow one to test under
harsh environmental conditions. Data analysis is basic and
produces results that are both reliable and comparable to
those obtained by others.

Using the double torsion test, average stress corrosion
factors of 96, 54 and 25 were obtained for specimens tested in
the dry, wet and hot wet environments, respectively. A
decrease in the stress corrosion factor of 45 percent was
observed between the dry and wet environments and a decrease
of 72 percent between the dry and hot wet environments. The
lower stress corrosion factor represents a greater material
sensitivity to stress corrosion cracking. Within any one
environment, the applied stress on the specimen was shown to
have no effect on the stress corrosion factor. Increasing or
decreasing the stress level caused only a parallel shift of
the curve to either the right or left, respectively.

Using the double torsion test stress corrosion cracking was
shown to be time dependent. During rapid load up, the loading

curves and initial load relaxations showed no environmental influence for the three cases. As relaxation continued increased load decay between the three environments was observed with time.

The same environmental influences were also observed in tests that were completed using one specimen subjected to both the dry and wet environments. These tests were conducted to eliminate specimen to specimen variation in material properties. When water was added to a specimen loaded in the dry condition a velocity change of over one order of magnitude was observed immediately.

Comparative tests on fracture toughness using fast loading rates and completed in the dry and wet environments showed almost no environmental influence.

Using the uniaxial compressive creep test, crack volume strains and crack volume strain rates were calculated for the dry and wet environments. In the dry environment no steady state creep was observed until 150 MPa. The creep rate at this load was approximately one fifteenth of the creep rate at the same load in the wet environment. The lowest creep rate measured in the wet environment was at a load of 126 MPa.

The stress dependence of the steady state creep rate for the

dry and wet environments was developed and fitted to several functions. A power function similar in form to the one used for the double torsion test fits both curves reasonably well. The hyperbolic function provides the best fit for the wet data, but predicts measurable creep rates in the 50 - 100 MPa range, which is not supported by the creep test data. The power function suggests measurable creep rates in the 120 MPa range which agrees quite well with the test data.

Using the crack volume strain rate data, time to failure predictions were made. Assuming a failure time of 1000 years and a critical crack volume of 1000 microstrain, the strength of LDB Granite in the wet environment works out to be 87 MPa. This represents slightly less than 40 percent of the dry mean instantaneous compressive strength. Static fatigue tests (Lajtai and Schmidtke, 1985) predicted a 1000 year strength of 120 to 140 MPa. The estimate derived from creep tests is based on time spent in steady state creep, which is representative of engineering projects measured in tens to hundreds of years. The life time predictions from long term creep tests therefore are more reliable than static fatigue tests which are based on tests only seconds to days in duration.

Microstructural and mineralogical control on crack growth was observed for both tensile and compressive loading. In tension

a major propagating crack can be observed with periods of
rapid growth over short distances followed by periods when the
crack front is stationary. Discontinuous crack formation
ahead of the main crack, propagation of parallel subcracks and
branching of the main crack can all be observed. Crack
advance occurs along grain boundaries (15 percent), cleavage
planes in microcline, oligoclase and biotite (60 percent) and
through complex fracture in quartz (25 percent). Microcline
and oligoclase offer the least resistance to crack growth,
quartz the most. The actual fracture path is approximately
twice as long as the straight line crack path. Crack
branching and secondary cracking is variable with ratios of
one to two times the straight line crack path.

Crack growth in compression is significantly different than in
tension. Cracks still take advantage of suitably oriented
planes of weakness, but the crack propagation direction for an
individual crack is usually within 10 degrees of the
compression axis. At low stress levels cracks generally grow
in feldspar grains. With increasing stress the density of
cracking increases as additional cracks develop parallel to
each other. As the stress reaches the failure point cracking
in quartz is the dominant process. Crack initiation and
arrest generally take place at quartz and biotite grains.

REFERENCES

Anderson, O.L., Stress-Corrosion Theory of Crack Propagation With Applications to Geophysics, Rev. Geophys. Space Phys. 15, 77-104, 1977.

Bezys, R., Fracture Initiation, Propagation and Arrest Produced by Compressive Loading and Unloading in the Lac du Bonnet Batholith, Unpublished B.Sc. Thesis, Department of Earth Sciences, University of Manitoba, 1984.

Bielus, L.P., Creep of Lac du Bonnet Granite Under Tension, Unpublished B.Sc. Thesis, Department of Geological Engineering, University of Manitoba, 1982.

Borynsky, L.C., Crack Advance in the Double Torsion Test, Unpublished B.Sc. Thesis, Department of Geological Engineering, University of Manitoba, 1983.

Boulton, J., Management of Radioactive Wastes: The Canadian Disposal Program, Atomic Energy of Canada Ltd. Report, AECL-6443, 1978.

Bruce, J.G., Gerberich, and W.W.,Koepke, B.G., Subcritical Crack Growth in PZT, Frac. Mech. Ceramics4, 687-709, 1978.

Charles, R.J., STatic Fatigue of Glass, J. Appl. Phys. 29, 1549-1560, 1959.

Denesiuk, B.E., Double Torsion Testing of Anorthosite, Unpublished B.Sc. Thesis, Department of Geological Engineering, University of Manitoba, 1983.

Evans, A.G., A Method for Evaluating the Time Dependent Failure Characteristics of Brittle Materialsand its Application to Polycrystalline Alumina, Journal of Materials Science 7, 1137-1146, 1972.

Harper, D.W., The Microstructural Control on the Strain Development of Lac du Bonnet Granite, Unpublished B.Sc. Thesis, Department of Geological Engineering, University of Manitoba, 1985.

Kies, .A., and Clark, A.B., Fracture Propagation Rates and imes to Fail Following Proof Stress in Bulk Glass, Procs. of the Second International Conference on Fracture, Paper 42, 1969.

Kranz, R.L., The Effects of Confining Pressure and Stress
Difference on Static Fatigue of Granite, J. Geophys. Res., 85,
1854-1866, 1980.

Lajtai, E.Z., Creep and Crack Growth in Lac du Bonnet Granite
Due to Compressive Stress, Fracture Problems and Solutions in
the Energy Industry, Procs. of the Fifth Can. Frac. Conf.,
229-238, 1981.

Lajtai, E.Z. and Bielus, L.P., Stress Corrosion of Lac du
Bonnet Granite in Tension and Compression, Rock Mechanics and
Rock Engineering 19, 71-87, 1986.

Lajtai, E.Z. and Schimdtke, R.H., Delayed Failure in Rock
Loaded in Uniaxial Compression, Int. Journal Rock Mechanics,
1985.

Matsui, M., Soma, T., and Oda, I., Subcritical Crack Growth in
Electrical Porcelains, Frac. Mech. Ceramics 4, 711-724, 1978.

McClintock, F.A., and Argon, A.S., Mechanical Behaviour of
Materials, Addison Wesley, 770p, 1966.

McRitchie, W.D., and Weber, W., Geology and Geophysics of the
Rice Lake Region, Southeastern Manitoba, Manitoba Mines Branch
Publication 71-1, 430p, 1978.

Penner, A.P., and Clark, G.S., b/Sr Age Determinations From
the Bird River Area, Southeastern Manitoba, G.A.C. Special
Paper #9, 105-109, 1971.

Ross, J.R., Microphotographic Anaalysis of Fracturing in Lac
du Bonnet Quartz Monzonite, Unpublished B.Sc. Thesis,
Department of Geological Engineering, University of Manitoba,
1982.

Svab, M. and Lajjtai, E.Z., Microstructural Control of Crack
Growth in Lac du Bonnet Granite, Fracture Problems and
Solutions in the Energy Industry, Procs. of the Fifth Can.
Frac. Conf., 219-228, 1981.

Swanson, P.L., Subcritical Crack Propagation in Westerly
Granite: An Investigation inti the Double Torsion Method, Int.
Journal of Rock Mechanics Mineral Sciences and Geomechanics
18, 445-449, 1981.

Tammemagi, H.Y., Kerford, P.S.,Requeima, J.C., and Temple,
C.A., A Geological Reconnaisance Study of the Lac du Bonnet
Batholith, Atomic Energy of Canada, AECL-6439, Pinawa,
Manitoba, 68p, 1980.

Tetelman, A.S., and McEvily, A.J., Fracture of Structural aterials, New York, Wiley and Sons, 1967.

Toshihiko, W., urta, K. and Misutani, H, The Effect of Water on Subcritical Crack Growth in Silicate Rocks, Tectonophysics 67, 25-64, 1980.

Wiederhorn, S.M., Stress Corrosion and Static Fatigue on Glass, Journal of the American Ceramic Society, 50, 407-415, 1967.

Wiederhorn, S.M., and Bolz, L.H., Stress Corrosion and Static Fatigue of Glass, Journal of the American Ceramic Society, 53, 544-548, 1970.

Wiederhorn, S.M., Mechanics of Subcritical Crack Growth in Glass, Frac. Mech. Ceramics, Vol. 4, New York, Plenum Press, 1978.

Williams, D.P., and Evans, A.G., A Simple Method for Studying Crack Growth, Journal of Testing and Evaluation, 1, 264-270, 1973.

Williams, D.P., and Nelson, H.G., Met. Trans., 1, 63, 1970.